Nonlocal electrodynamics of long ultranarrow Josephson junctions: Experiment and theory

A. A. Abdumalikov, Jr.,[1,*] V. V. Kurin,[2] C. Helm,[3] A. De Col,[3] Y. Koval,[1] and A. V. Ustinov[1]

[1]*Physikalisches Institut III, Universität Erlangen-Nürnberg, Erlangen D-91058, Germany*
[2]*Institute for Physics of Microstructure (RAS), Nizhniy Novgorod, Russia*
[3]*Institut für Theoretische Physik, ETH Hönggerberg, Zürich 8093, Switzerland*

We experimentally and theoretically investigate electromagnetic cavity modes in ultranarrow Al-AlO$_x$-Al and Nb-AlO$_x$-Nb long Josephson junctions. Experiments show that the voltage spacing between the Fiske steps on the current-voltage characteristics of sub-μm-wide and several hundred μm-long Al-AlO$_x$-Al and Nb-AlO$_x$-Nb Josephson junctions increases when decreasing the junction width. This effect is explained by stray magnetic fields, which become important for narrow junctions. Theoretical estimates of the Fiske step voltage based on a nonlocal wave propagation equation are in agreement with our experimental data. Using the nonlocal model, we determine the size and mass of a Josephson vortex by means of a variational approach, and relate the vortex size to the experimentally measured critical magnetic field of the junction.

I. INTRODUCTION

The electromagnetic properties of Josephson tunnel junctions have been the subject of intensive studies over the past four decades.[1–4] Most investigations of the junction dynamics have been based on local theory. This theory assumes that electromagnetic fields are concentrated within the junction barrier, and neglects the distribution of the magnetic and electric fields outside the junction. However, in reality, the fields penetrate the superconducting electrodes and extend into free space (Fig. 1). Local theory breaks down when the fields outside the junction contribute significantly to the junction energy. In both cases the wave equation describing the junction becomes nonlocal.

The energy of the magnetic field inside the superconducting electrodes of a Josephson junction becomes considerable when the London penetration depth λ_L is of the order of, or larger than, the Josephson penetration depth λ_J. The Josephson penetration depth characterizes the scale of spatial variations of the phase difference φ between the wave functions of the superconducting electrons in each electrode of the junction, also called the Josephson phase. This type of non-locality we call *internal*, because it only depends on the field distribution inside the junction and its electrodes, and neglects extended stray fields outside the junction.

When the energy of the stray fields becomes comparable to the energy of the field inside the junction, one has to take the stray fields into account. These stray fields generate an additional surface current $\mathbf{J}_S$, which can be represented as a functional of the magnetic-field distribution inside the junction, leading to a nonlocal equation. Because these effects depend on the geometry of the junction, we call them *geometrical nonlocal* effects.

Detailed knowledge of Josephson vortex dynamics is important in understanding magnetic flux motion and related phenomena in superconductors. In a junction which is long compared to the Josephson penetration depth λ_J, a vortex behaves like a classical particle, and is characterized by its effective mass and its spatial coordinate. The interest in experimentally verifying theoretically predicted nonlocal cor-

rections to the conventional model has grown due to recent studies of long ultranarrow junctions where Josephson vortices behave as macroscopic quantum objects.[5,6] In very narrow junctions, the *effective dynamical mass* of the vortex is expected to be influenced by stray magnetic fields. Most theoretical studies assume, however, that the effective dynamical mass of a Josephson vortex is proportional to the width of the junction as expected from local theory.[7–9] Note that the mass of a vortex corresponds to the static energy of a junction containing one vortex, see Sec. IV E.

In this paper we experimentally verify that, for very narrow long Josephson junctions, one must take into account the vortex mass correction due to the stray fields outside the junction. Significant deviations from local theory have previously been observed in the current-voltage characteristics of long junctions of small width.[10] Here, we systematically study these effects for different junction materials, and compare the experimental findings with the nonlocal sine-Gordon model.

A Josephson junction can be considered quasi-one-dimensional as long as its transverse dimension, the width w in the z direction (see Fig. 1), is smaller than the Josephson penetration depth
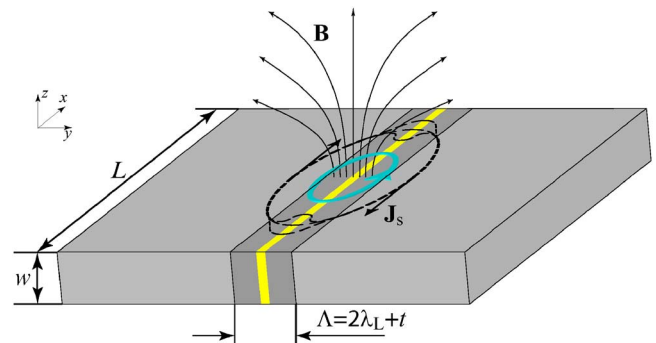

FIG. 1. (Color online) Schematic view of an edge-type long Josephson junction of width w and length L. The lines show the magnetic field **B**, due to vortex (solid blue line), which penetrates the electrodes and extends into free space. The extended stray magnetic field creates the additional surface current $\mathbf{J}_S$ (dashed line).

$$\lambda_J = \sqrt{\frac{\Phi_0}{2\pi\mu_0 j_c \Lambda}}, \quad (1)$$

where Φ_0 is the magnetic-flux quantum, j_c is the critical current density across the tunnel barrier, $\Lambda = 2\lambda_L + d$ is the magnetic thickness of the junction, and d is the barrier thickness (typically, $d \ll \lambda_L$). In this limit ($w \ll \lambda_J$), the dynamics of a long junction are described by the one-dimensional perturbed sine-Gordon equation for the Josephson phase φ,

$$\lambda_J^2 \varphi_{xx} - \omega_p^{-2} \varphi_{tt} - \omega_p^{-1} \alpha \varphi_t - \sin\varphi = -\gamma, \quad (2)$$

where subscripts denote partial derivatives with respect to time t and the spatial coordinate x along the junction. The parameter

$$\omega_p = \sqrt{\frac{2\pi j_c}{\Phi_0 C}} \quad (3)$$

is the Josephson plasma frequency, C is the specific capacitance of the junction per unit area, and α is the dissipation coefficient due to the quasiparticle tunneling across the barrier. The bias current density $\gamma = j/j_c$ is normalized to the critical current density j_c, and in general depends on x.

Equation (2) is derived using the following assumptions: (i) $\lambda_L \ll w \ll \lambda_J$ and (ii) $\hbar\omega \ll \Delta$, where ω is the oscillation frequency of the phase φ, and Δ is the superconducting energy gap of the electrodes. The breakdown of any of these conditions requires modification of Eq. (2). As mentioned above, for large London penetration depths $\lambda_L \gtrsim \lambda_J$, or small Josephson penetration depths λ_J, the magnetic field inside the superconductor starts to play an important role. On the other hand, for sufficiently small junction widths $w \sim \lambda_L$, the stray fields outside the junction have to be taken into account. In either case, the dynamics of the phase φ has to be described by an integrodifferential equation, i.e., the problem becomes nonlocal. When the oscillation frequency ω is comparable to the superconducting gap Δ, the frequency dependence of the London penetration depth $\lambda_L(\omega)$ given by the microscopic theory, *material dispersion*, should also be taken into account.[11–13]

The nonlocal equation describing Josephson phase dynamics can be written in general form as

$$\lambda_J^2 \frac{\partial}{\partial x} \int dx' Q(x,x') \varphi_{x'}(x') - \omega_p^{-2} \varphi_{tt} - \omega_p^{-1} \alpha \varphi_t - \sin\varphi = \gamma,$$

$$(4)$$

where the function $Q(x,x')$ is the nonlocality kernel, which needs to be specifically determined for each nonlocal problem. In the local case $Q(x,x') = \delta(x-x')$, where $\delta(x)$ is a delta function. Several theoretical approaches have been proposed for different types of nonlocality in the case of an infinitely long Josephson junction. In this limit the kernel of the integral in Eq. (4) is reduced to the function of a single argument, $Q(x,x') = Q(|x-x'|)$.

Nonlocal models can be divided into two groups: those treating internal nonlocality inside bulk junctions,[14,15] and those dealing with nonlocal effects due to external stray fields resulting from the geometry of the junction and its
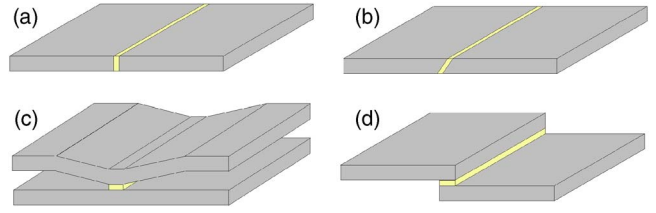

FIG. 2. (Color online) Different geometries of long Josephson junctions formed between two superconducting films: (a) edge-type junction; (b) ramp-type junction; (c) window junction; (d) overlap junction.

electrodes.[16–29] The latter group of theories takes into account the field configuration not only inside the junction, but also around it, and incorporates the finite size of the sample and its shape-dependent magnetic properties. The shorter the junction is in the x direction (see Fig. 1), or the narrower it is in the z direction, the larger the effect of the geometrical nonlocality. Four typical geometries of long Josephson junctions are presented in Fig. 2. These are (a) edge-type, (b) ramp-type, (c) window, and (d) overlap long junctions. In the ideal case of an infinitely long junction, the electrodynamic problem posed by the (a)–(c)-type junctions have been solved. In particular, theoretical models for geometrical nonlocality have analyzed the following cases: (i) edge-type junctions between thick films $w \gtrsim \lambda_L$, neglecting internal nonlocal effects;[21,29] (ii) edge-type junctions between thin films $w < \lambda_L$ (Pearl's limit);[18,28,30] (iii) edge-type and (iv) ramp-type junctions between films of arbitrary width, taking into account both the internal and external nonlocal problems;[24,25] (v) a variable thickness bridge above a ground plane;[16,17] and (vi) window junctions.[20,26,27]

In this paper, we study the effect of geometrical nonlocality by analyzing experiments on extremely narrow long Josephson junctions of width down to 0.1 μm. In Sec. II we describe the geometries and preparation process of ultranarrow low-T_c long Josephson junctions. In Sec. III we present experimental results obtained for Nb-AlO$_x$-Nb and Al-AlO$_x$-Al junctions. Theoretical models based on nonlocal electrodynamics are briefly reviewed in Sec. IV A, and their comparison with experiment is presented in Secs. IV C and IV D. In Sec. IV E we calculate the mass of a vortex, and thus the energy of a junction in the nonlocal limit. Section V contains concluding remarks.

II. FABRICATION AND GEOMETRY OF ULTRANARROW LONG JOSEPHSON JUNCTIONS

The fabrication process of high quality long Josephson junctions in order to study the effects of nonlocal electrodynamics should satisfy the following three requirements: (i) ability to vary the junction width from several micrometers down to several hundred nanometers, (ii) constant width along the junction length $L \gg \lambda_J$, which is typically several hundred micrometers, and (iii) an idle area of overlapping electrodes (window) that is as small as possible, so as to prevent it influencing wave propagation in the junction. We prepared samples using two different technologies based on
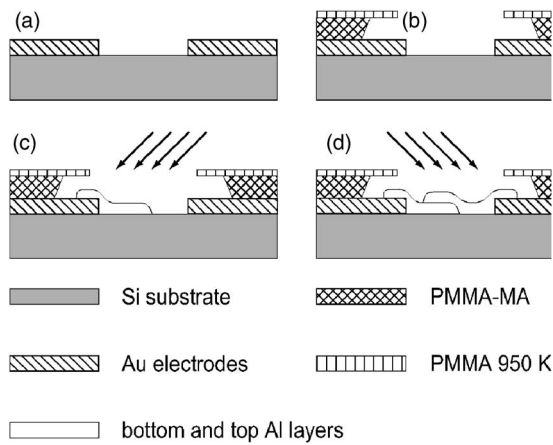
FIG. 3. Schematic diagram of the fabrication procedure for Al junctions. (a) Deposition of Au electrodes; (b) formation of a window in the PMMA resist for shadow evaporation; (c), (d) deposition of top and bottom Al electrodes.

FIG. 5. Schematic cross sections of experimentally studied Al-AlO$_x$-Al (a) and Nb-AlO$_x$-Nb (b) junctions.

aluminium and niobium. All samples were fabricated on thermally oxidized Si substrates.

A. Al-AlO$_x$-Al junctions

The Al-AlO$_x$-Al junctions were prepared with the shadow evaporation technique. This method for the preparation of sub-μm Al-AlO$_x$-Al tunnel junctions is well known (see, e.g., Ref. 31). However, we cannot apply this method directly. A suspended bridge of electron resist (e.g., PMMA) or another material is usually used for shadowing during the evaporation of Al. As the length of the bridge becomes longer the bridge starts to sag. Thus for fabrication of long junctions (several hundred micrometers) the suspended bridge technique cannot be used. Therefore, in our preparation method, we use an alternative method based on a *shadowing window*. Schematically, the fabrication steps are shown in Fig. 3.

The first step is the formation of Au electrodes, used for spatially uniform bias current injection and voltage measurement leads [Fig. 3(a)]. These electrodes are formed with the help of electron-beam lithography, thermal evaporation, and the lift-off technique. The Ti layer under the Au layer improves Au adhesion to the substrate. The thicknesses of the Ti and Au layers were 10 and 50 nm, respectively. The elec-
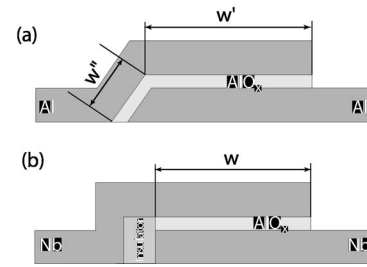
trodes for current injection and voltage measurement across the junction have different geometries. One sees in Fig. 4 that the bias current leads have a width approximately equal to that of the Josephson junction. The voltage measurement leads are much smaller, and are connected to the junction only at the edges of the Al electrodes. This geometry provides homogeneous current injection into long Josephson junctions and allows four-point measurements of their characteristics.

To form a long Josephson junction by shadow evaporation, we used double layer resist PMMA-MA/PMMA 950 K, which was spanned onto the substrate with prepared Au/Ti electrodes. Then, using electron-beam lithography, we opened a window between the Au/Ti electrodes, as shown in Fig. 3(b). In the next step, we evaporated Al onto a tilted substrate [see Fig. 3(c)]. The thickness of this bottom Al layer was about 100 nm. Immediately after Al evaporation O$_2$ was injected into the vacuum chamber. The pressure of O$_2$ was kept at 5×10^{-2} mBar for 5 min. Then, a 105-nm-thick top layer of Al was evaporated onto the tilted substrate [Fig. 3(d)]. The overlap of the bottom and top Al electrodes defines the junction area. A scanning electron micrograph of the resulting Josephson junction and electrodes is shown in Fig. 4.

Schematically, the cross section of the fabricated Josephson junction is shown in Fig. 5(a). Note that the total junction width is composed of two sections, one, of width w', parallel to the film surface plane and another, of width w'', which is tilted. The total width is therefore $w = w' + w''$. Typically the relation $w'' \ll w'$ is well fulfilled. However, in the case of the most narrow junctions, the contribution of w'' to the junction width becomes significant. We estimate $w'' \simeq 100$ nm.
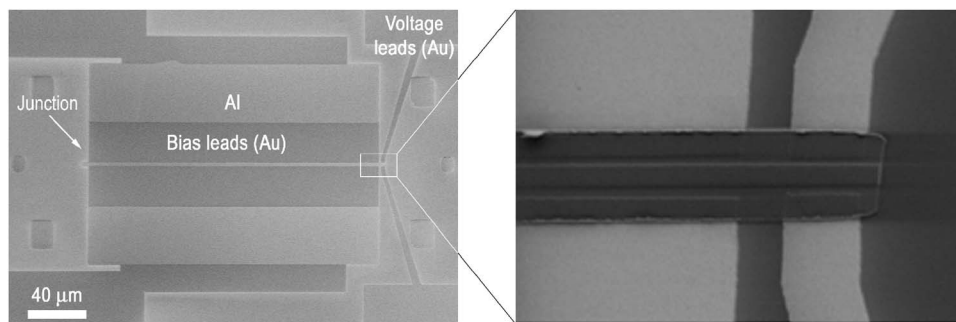

FIG. 4. SEM picture of Al-AlO$_x$-Al junction. The inset shows an enlarged view of the connection of current and potential electrodes to the junction.
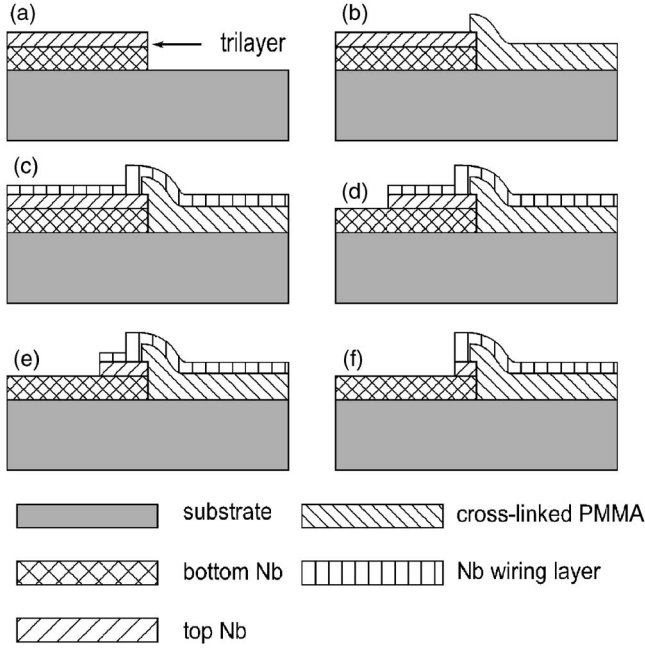
FIG. 6. Schematic diagram of the fabrication procedure for Nb junctions. (a) Formation of the trilayer; (b) insulation of the trilayer edge; (c) deposition of Nb wiring; (d) removal of Nb wiring and top Nb from all areas except that of the junction, (e), (f) narrowing of the junction using electron beam lithography and reactive ion etching (repeated several times).

B. Nb-AlO$_x$-Nb junctions

There are several different approaches for the preparation of Josephson junctions using Nb-AlO$_x$-Nb trilayer technology. They differ mainly in patterning and insulation of the junction. Junctions with dimensions less than 1 μm usually have a window geometry [see Fig. 2(c)], and are produced by reactive ion etching and vapor deposition of a dielectric layer. Using this approach, one could prepare sub-μm junctions, however, they would not satisfy the requirement of small idle region between the superconducting electrodes around the junction. In our group, we demonstrate an alternative method, which allows junctions to be produced on the very edge of the Nb-AlO$_x$-Nb trilayer.[10] Schematically, this process is shown in Fig. 6. The junction cross section prepared in this way is shown in Fig. 5(b).

In the first step, the Nb-AlO$_x$-Nb trilayer region is defined by lithography and reactive ion etching [Fig. 6(a)]. The next step is the fine definition of one of the edges of the structure using electron-beam lithography and etching. This particular edge was insulated by cross-linked PMMA [see Fig. 6(b)]. The details of the cross-linking procedure and the self-alignment of cross-linked PMMA along the trilayer edge can be found in Ref. 10. In the next step, the Nb wiring layer was deposited as shown in Fig. 6(c). Electron-beam lithography and reactive ion etching were used to define the junction area [see Fig. 6(d)]. After performing a full set of measurements on the junction, the width of the junction was iteratively decreased using electron beam lithography and reactive ion etching, as shown in Figs. 6(e) and 6(f).

Using this process we fabricated a wide junction of width 4.2 μm, and decreased width in steps down to 300 nm. The

TABLE I. Parameters of the measured junctions.

Electrode material	λ_L, nm	J_c, A/cm^2	λ_J, μm	$\bar{c}$, m/s	V_{gap}, mV
Al (T=0.3 K)	105	500	16	5×10^6	0.35
Nb (T=4.2 K)	90	210	25	7×10^6	2.7

critical current and the normal resistance of the junction, after the RIE process, scales with its width.[10]

III. EXPERIMENT

In this section, we present the data acquired for Al-AlO$_x$-Al and Nb-AlO$_x$-Nb ultranarrow long Josephson junctions. A magnetic field H of up to 40 Oe was applied in the plane of the junction, perpendicular to its longer dimension. The magnetic field of the Earth was screened out by a cryoperm shield. The experimentally determined parameters of the junctions are summarized in Table I. The London penetration depths for Al and Nb were found from the period ΔH of the $I_c(H)$ dependence at high fields using junctions of length 10 μm, as $\lambda_L = \Phi_0/(2L\Delta H)$. The Josephson penetration depth was obtained from the critical current density using Eq. (1). The Swihart velocity was found by fitting Fiske step voltages to the theoretical dependence (see Sec. IV C). The junction width was measured using a scanning electron microscope.

In the following, we describe two major effects observed in our ultranarrow Josephson junctions, which occur when the junction width w is decreased. These are (i) a reduction in the first critical field H_{c1}, and (ii) an increase of the Fiske step voltage spacing ΔV_{FS}. According to standard local theory, the first critical field H_{c1} and the Fiske step voltage should not depend on the junction width.[2]

The first critical field corresponds to the field when a single vortex enters the junction. In the local theory, the first critical field H_{c1} is inversely proportional to the Josephson penetration depth λ_J. In the following sections we present the experimental data for H_{c1} in terms of characteristic length

$$\widetilde{\lambda}_J = \frac{\Phi_0}{\pi H_{c1}(2\lambda_L + d)}. \tag{5}$$

Note that this equation is similar to the relation between λ_J and H_{c1} in the local theory.

Fiske steps arise when the Josephson oscillation frequency resonates with cavity modes of the junction. According to local theory, the voltages of these steps are given by[2]

$$V_n = \frac{\Phi_0}{2\pi} \frac{n\pi}{L} \bar{c}, \tag{6}$$

where $\bar{c}$ is the Swihart velocity and n is the step number.

A. Al-AlO$_x$-Al junctions

We measured a series of ten 230-μm-long Al-AlO$_x$-Al junctions. The width w of the junctions varied between 0.1 and 1.3 μm. The homogeneity of the junctions was verified by measuring the modulation pattern of the critical current I_c
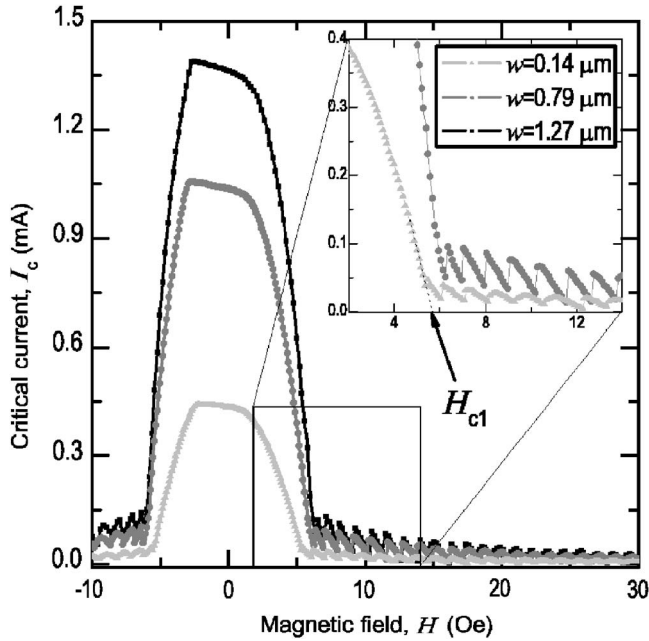
FIG. 7. Critical current modulation $I_c(H)$ in magnetic field for long Al-AlO$_x$-Al Josephson junctions at $T = 0.9$ K. The inset zooms in on the modulation patterns of the junctions of width $w = 0.14$ μm and $w = 0.79$ μm.

vs field H at $T = 0.3$ K. In Fig. 7, $I_c(H)$ patterns of three samples of width $w = 0.14$, 0.79, and 1.27 μm are presented. We find the first critical field by linearly extrapolating the central peak in the critical current modulation pattern (see the inset of Fig. 7). We observe that the first critical field H_{c1} increases with the junction width w. Note that the measured $I_c(H)$ patterns are slightly tilted due to small asymmetry of the junction bias leads, see Fig. 4. The flatness of the central $I_c(H)$ maximum is due to the heating effect of the normal Au/Ti electrodes.

The characteristic length $\widetilde{\lambda}_J$ experimentally determined using Eq. (5) is presented in Fig. 8 as black squares. One can see that it strongly depends on the junction width. Theoretical curves are discussed below, in Sec. IV D.

Fiske steps of all junctions were measured by tracing the current-voltage characteristics during a continuous sweep of the external field H in the range from -40 to $+40$ Oe. In Fig. 9, superimposed characteristics are plotted for the junction of width $w = 0.79$ μm.

We have observed that the positions of the Fiske steps strongly depend on the width of the junction. This dependence for the first step is shown in Fig. 10 and compared with the theory presented below in Sec. IV C.

B. Nb-AlO$_x$-Nb junctions

Results of systematic measurements of ten long narrow Nb-AlO$_x$-Nb junctions were presented earlier in Ref. 10. We have now additionally measured three more junctions. Measurements were performed at temperature $T = 4.2$ K. In the present paper we analyze earlier data and our new results more extensively. The junction length is 200 μm and the

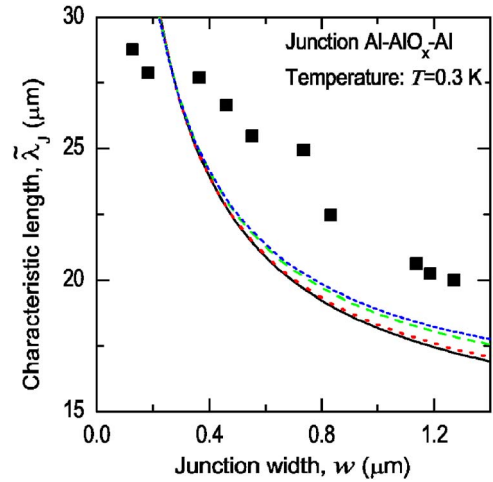FIG. 8. (Color online) Characteristic length $\widetilde{\lambda}_J$ for Al-AlO$_x$-Al junctions. Squares indicate $\widetilde{\lambda}_J$, extracted from the measured critical field H_{c1} at temperature $T = 0.3$ K, using Eq. (5). Lines show theoretical estimations of $\widetilde{\lambda}_J$, for details see Sec. IV D.

width w ranges from 0.3 to 4.25 μm. The Josephson penetration depth was estimated from the critical current density using Eq. (1) to be about $\lambda_J \approx 25$ μm. The critical current vs magnetic field patterns, reported in Ref. 10, and those of the new junctions show that all junctions are rather homogeneous. As in the case of the Al-AlO$_x$-Al junctions, a decrease in the first critical field H_{c1} (Fig. 11), and an increase in the Fiske step voltage spacing ΔV_{FS} (Fig. 12), with decreasing width w were observed in the Nb-AlO$_x$-Nb junctions.

IV. COMPARISON WITH THEORY

In this section, we present a short review of existing theoretical models for nonlocal effects in edge-type Josephson junctions (Fig. 1). In particular, we are interested in the non-
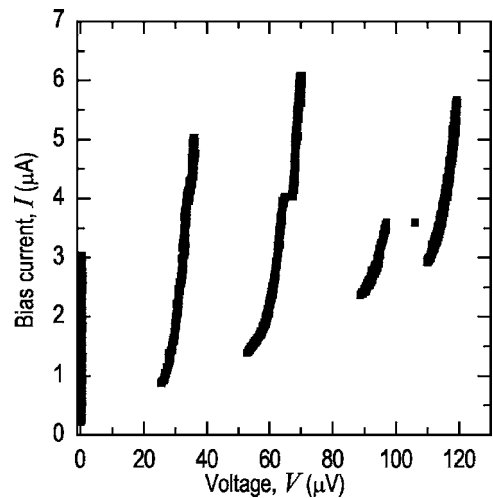

FIG. 9. Superimposed traces of Fiske resonances of the current-voltage characteristics of Al-AlO$_x$-Al long Josephson junctions at several different magnetic fields. The junction width is $w = 0.79$ μm and the temperature is $T = 0.3$ K.
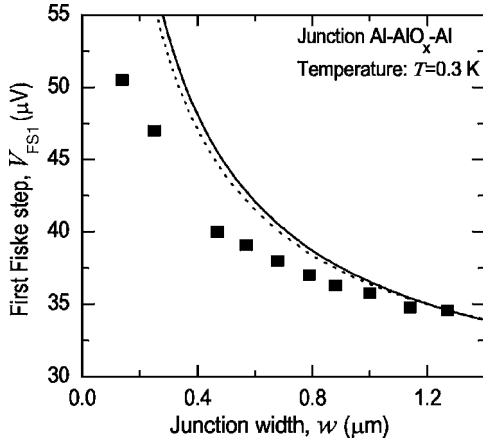
FIG. 10. The width dependence of the first Fiske step voltage V_1 for Al-AlO$_x$-Al junctions. Symbols correspond to experimental data obtained at $T=0.3$ K. Lines correspond to the theoretical models of edge-type junctions which neglect internal nonlocality (Ref. 21) (solid), and to the more general theory describing both internal and geometrical nonlocal effects (Ref. 24) (dashed).

local kernels $Q(x,x')$ to be used in Eq. (4), and in the dispersion relation $\omega(k)$ of the junction, which determines the voltage position V_n of Fiske resonances. To compare with the experimental data, we include the frequency dependence of $\lambda_L(\omega)$ due to material dispersion, and relate the critical magnetic field H_{c1} to the effective size of a vortex.

A. Geometrical Nonlocality

In a junction of finite length L the translational invariance along the junction is broken and, in general, the kernel $Q(x,x')$ depends not only on $x-x'$, but also on the sum $x+x'$ and the length L. However, in a finite junction, deviations of the nonlocality kernel from the one of an infinitely
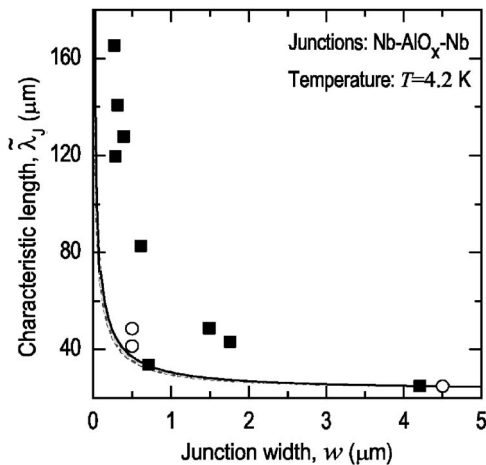

FIG. 11. Characteristic length $\tilde{\lambda}_J$ for Nb-AlO$_x$-Nb junctions at $T=4.2$ K. The open circles denote the characteristic length $\tilde{\lambda}_J$ extracted from the experimental critical field H_{c1} according to Eq. (5) for our more recent junctions. The solid symbols correspond to experimental data for H_{c1} from Ref. 10. Lines correspond to theoretical estimations of $\tilde{\lambda}_J$ (see Sec. IV D).
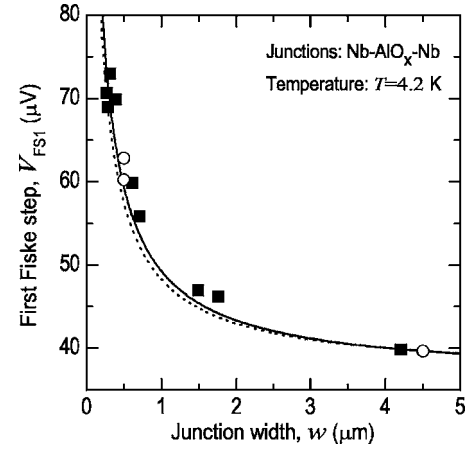

FIG. 12. The width dependence of the maximum of the first Fiske step voltage V_1 for Nb-AlO$_x$-Nb junctions. The open symbol corresponds to new experimental data, while the data for solid symbols are taken from Ref. 10. The solid line corresponds to the theoretical model for edge-type junctions which neglects internal nonlocality (Ref. 21), while the more general theory describing both internal and geometrical nonlocal effects (Ref. 24) corresponds to the dashed line.

long junction are expected, mainly in the edge region on the order of the London penetration depth λ_L (or $\lambda_P=2\lambda_L^2/w$ in thin films). These deviations can be neglected for junctions of length $L \gg \lambda_L$ ($L \gg \lambda_P$), as considered in the following.

We distinguish between nonlocal effects due to stray fields and screening currents inside and outside the junction electrodes. These two contributions are referred as internal and geometrical nonlocality, respectively.

(a) Let us first consider the theory for internal nonlocal effects in bulk junctions of width $w \gg \lambda_L$, see Refs. 14 and 15. In this case the kernel in Eq. (4) is

$$Q(x) = (1/\pi\lambda_L)K_0(|x|/\lambda_L), \tag{7}$$

where K_0 is a modified Bessel function, having a logarithmic pole at $x \to 0$ and exponentially decaying at large distances.[32] Therefore internal nonlocal effects become important when λ_L is large compared to the Josephson penetration depth λ_J, on which the phase varies, i.e., in the case of $\lambda_L \gtrsim \lambda_J$. In the limit $\lambda_L \ll \lambda_J$ the local sine-Gordon equation is recovered.

Usually λ_J is much larger than λ_L, because the critical current density j_c in the junction is much smaller than the critical depairing current density $j_d=2\Phi_0/(3\sqrt{3}\pi^2\mu_0\lambda_L^2\xi)$ in the bulk superconductor, where ξ is the coherence length. Exceptions are, for example, junctions in high-temperature superconductors created by planar defects such as twins, stacking faults, low-angle grain boundaries, etc.[33] These structural defects often form Josephson junctions with high j_c and therefore small λ_J. In terms of the critical current density across the junction, the condition $\lambda_J < \lambda_L$ is fulfilled if $j_d/\kappa < j_c < j_d$, where $\kappa = \lambda_L/\xi$ is the Ginzburg-Landau parameter.[14] Note that for extreme type-II superconductors, $\kappa \gg 1$, and the relation $\lambda_J < \lambda_L$ holds over a wide range of j_c.

Linearizing the wave equation (4) ($\sin\varphi \simeq \varphi$), one obtains the dispersion relation $\omega(k)$ for small-amplitude linear elec-

tromagnetic waves $\varphi(x,t) = \varphi_0 \exp(-i\omega t + ikx)$ (here $|\varphi_0| \ll 1$) propagating along a Josephson junction. From the above kernel it follows that

$$\omega = \omega_p \left(1 + \frac{k^2\lambda_J^2}{\sqrt{1+k^2\lambda_L^2}} \right)^{\frac{1}{2}}. \tag{8}$$

(b) The geometrical nonlocality of an edge-type junction formed between two thin superconducting films of width $w < \lambda_L$ [Fig. 2(a)] has been extensively studied.[18,22,28] In this case, the stray fields outside the junction area account for the entire electromagnetic energy of the junction. In thin films, the typical length scale upon which magnetic fields vary is not the London penetration depth λ_L, but the Pearl penetration depth[30] $\lambda_P = 2\lambda_L^2/w \gg \lambda_L$. The nonlocality kernel is then given by[28]

$$Q(x) = \frac{4\lambda_L}{w} \int \frac{dk \, dq}{(2\pi)^2} \frac{\exp(ikx)}{\sqrt{k^2+q^2}[1+\lambda_P^2 q^2]}$$
$$= \frac{1}{2\lambda_L} \left[\mathbf{H}_0\left(\frac{|x|}{\lambda_P}\right) - Y_0\left(\frac{|x|}{\lambda_P}\right) \right], \tag{9}$$

where $\mathbf{H}_0$ and Y_0 are the Struve and Bessel function of the second kind.[32] As in the previous case, this kernel has a logarithmic pole at $x \to 0$, however, at large distances it decays as $1/x$. When the characteristic length $\widetilde{\lambda}_J$, on which Josephson phase φ changes, is large compared to the Pearl penetration depth, $\lambda_P \ll \widetilde{\lambda}_J$, it is given by $\widetilde{\lambda}_J = \lambda_J(\lambda_L/w)^{1/2} \gg \lambda_J$. The limit of $\lambda_P \ll \widetilde{\lambda}_J$ is then equivalent to $\lambda_L \ll \lambda_J(w/\lambda_L)^{1/2}$.

(c) Ivanchenko's theory[21] applies to edge-type junctions of width larger than the London penetration depth, $w \gtrsim \lambda_L$. This model assumes that stray fields outside the film affect only the surface, and that the interior of the junction is described by the local theory. In this case the integral kernel has the form[21]

$$Q(x) = \delta(x) + \frac{4\lambda_L}{w} \int \frac{dk \, dq}{(2\pi)^2} \frac{\exp(ikx)}{\sqrt{k^2+q^2}[1+\lambda_L^2 q^2]}$$
$$= \delta(x) + \frac{1}{w} \left[\mathbf{H}_0\left(\frac{|x|}{\lambda_L}\right) - Y_0\left(\frac{|x|}{\lambda_L}\right) \right]. \tag{10}$$

Note that the second term is identical to the kernel of Eq. (9), corresponding to the case of a thin-film junction, but the Pearl penetration depth λ_P is replaced by the London penetration depth λ_L. As in the previous case, when the characteristic length $\widetilde{\lambda}_J$ is large compared to the size of the kernel, $\lambda_L \ll \widetilde{\lambda}_J$, it is given by $\widetilde{\lambda}_J = \lambda_J(1+\lambda_L/w)^{1/2}$.

In the limit of $\widetilde{\lambda}_J \gg \lambda_L$ for cases (b) and (c), Eq. (4) does not transform into the local sine-Gordon equation with characteristic length $\widetilde{\lambda}_J$, because $Q(x)$ does not correspond to $\delta(x)$ for $\lambda_{P/L} \to 0$. Nevertheless, the locality of the kernel suggests that in this limit an effective local sine-Gordon equation with renormalized Josephson penetration depth $\widetilde{\lambda}_J$

should be qualitatively correct. Then one could use the expression for H_{c1} from local theory, if λ_J is replaced by a new length $\widetilde{\lambda}_J$, see below.

In the absence of dissipation and bias current, using the kernel (10) we obtain the dispersion relation

$$\omega(k) = \omega_p \sqrt{1 + k^2\lambda_J^2 + \frac{4k^2\lambda_J^2\Lambda}{\pi w\sqrt{k^2\Lambda^2-4}} \arccos\left(\frac{2}{|k|\Lambda}\right)} \tag{11}$$

for $k\Lambda \geq 2$ and

$$\omega(k) = \omega_p \sqrt{1 + k^2\lambda_J^2 + \frac{4k^2\lambda_J^2\Lambda}{\pi w\sqrt{4-k^2\Lambda^2}} \text{arccosh}\left(\frac{2}{|k|\Lambda}\right)} \tag{12}$$

for $k\Lambda < 2$.

(d) The theory developed by Lomtev and Kuzovlev[24] is the most general as it contains the special cases (a)–(c) discussed above. It assumes that the phase $\varphi(x)$ does not vary over the width w. The kernel is

$$Q(x) = \frac{1}{\pi\lambda_L} K_0\left(\frac{|x|}{\lambda_L}\right) + \frac{2}{\pi w\lambda_L^3} \int_0^\infty \frac{dq J_0(qx)}{\kappa^3[\kappa + q\coth(\kappa w/2)]}, \tag{13}$$

where $\kappa = (q^2 + \lambda_L^{-2})^{1/2}$, and J_0 is the Bessel function of the first kind. In this case the dispersion relation in the absence of perturbation terms in Eq. (4) is[24]

$$\omega(k) = \omega_p \sqrt{1 + \frac{k^2\lambda_J^2}{\sqrt{1+k^2\lambda_L^2}} + \frac{k^2\lambda_J^2}{\pi\lambda_L}F(k)}, \tag{14}$$

where

$$F(k) = \frac{2}{w\lambda_L^2} \int_k^\infty dq \frac{1}{\kappa^3} \frac{1}{\kappa + k\coth(\kappa w/2)} \frac{1}{(q^2-k^2)^{1/2}}. \tag{15}$$

This theory has also been generalized to describe ramp-type junctions[25] [Fig. 2(b)].

Let us quote typical parameters for our low-T_c long Josephson junctions. For the Nb-AlO$_x$-Nb junctions considered in this paper $\lambda_J \simeq 25$ μm and $\lambda_L \simeq 90$ nm at $T = 4.2$ K, and for Al-AlO$_x$-Al junctions $\lambda_J \simeq 16$ μm and $\lambda_L \simeq 105$ nm at $T = 0.3$ K. For these parameters, the condition $\lambda_L \ll \lambda_J$ is fulfilled in all cases, i.e., the internal nonlocal effects as discussed in case (a) are negligibly small. For Al-AlO$_x$-Al junctions the width $w \approx 0.1$–1.3 μm, and for Nb-AlO$_x$-Nb junctions the width $w \approx 0.3$–4.2 μm, which are larger than λ_L. It is reasonable to expect that our junctions can be approximately described by the theory presented in Ref. 21. In the following analysis, we compare our experimental data with Ivanchenko's theory,[21] case (c), and with the more general theory of Lomtev and Kuzovlev,[24] case (d).

B. Material dispersion

We will see in Sec. IV C that for small frequencies the nonlocal dispersion relation predicts a strong decrease of the

spacing between the Fiske steps $\Delta V_{FSn} = V_n - V_{n-1}$ with increasing n [cf. Eqs. (11), (12), (14), and (21)]. For large wave numbers, this effect is of the same order of magnitude as the reduction of the spacing between Fiske steps due to material dispersion.[12] Material dispersion arises from the frequency dependence of the complex conductivity and surface impedance of the superconducting electrodes.[11,13] It leads to a frequency dependence of λ_L which becomes significant at frequencies on the order of the superconducting energy gap frequency $f_{gap} = \Delta/h$, where Δ is the superconducting energy gap. The gap frequency of the Nb-AlO$_x$-Nb junctions is $f_{gap} \simeq 650$ GHz (at 4.2 K) and that of Al-AlO$_x$-Al is $f_{gap} \simeq 85$ GHz (at 0.3 K). The frequency dependence of λ_L can be written as[11,12]

$$\left(\frac{\lambda_L(0)}{\lambda_L(\omega)}\right)^2 = \sqrt{\pi\Delta}\int_{\Delta-\hbar\omega}^{\Delta} dx [1-2f(x+\hbar\omega)]$$
$$\times \frac{x^2 + \Delta^2 + x\hbar\omega}{\sqrt{\Delta^2 - x^2}\sqrt{(x+\hbar\omega)^2 - \Delta^2}}, \qquad (16)$$

where $f(x) = 1/(1+e^{x/k_B T})$ is the Fermi-Dirac distribution function, and k_B is Boltzmann's constant.

C. Fiske steps

Let us consider a long junction of length L. Because of reflection at the edges, it behaves like a resonant transmission line for cavity modes of the electromagnetic field. The theory of such resonances (Fiske resonances) in the local case was developed by Kulik.[34,35] The nonlocal theory for semi-infinite, and finite Josephson junctions [19,36] suggest that for case (c) of Ivanchenko,[21] in the presence of an external magnetic field H_e, we can use the boundary condition

$$\varphi_x(0) = \varphi_x(L) = \frac{2\pi\Lambda}{\Phi_0}H_e. \qquad (17)$$

Then, the Josephson phase is written as

$$\varphi = \omega t - kx + \varphi_1(x,t), \qquad (18)$$

where $\omega = 2\pi V/\Phi_0$ and $k = 4\pi\lambda_L H_e/\Phi_0$. As a first approximation, we consider $\varphi_1(x,t)$ as a small perturbation. By inserting this into Eq. (4) we obtain

$$\lambda_j^2 \frac{\partial}{\partial x}\int dx' Q(x-x')\varphi_{1,x'}(x') - \omega_p^{-2}\varphi_{1,tt} - \omega_p^{-1}\alpha\varphi_{1,t}$$
$$= \sin(\omega t - kx), \qquad (19)$$

where we neglect $\varphi_1(x,t)$ in the sine term, and use the assumption concerning the nonlocality kernel made at the beginning of Sec. IV A. Further, $\varphi_1(x,t)$ can be expanded in terms of the normal modes of the junction

$$\varphi_1(x,t) = \mathrm{Im}\left\{\sum_{n=0}^{\infty} g_n e^{i\omega_n t}\cos k_n x\right\}, \qquad (20)$$

where g_n are complex numbers, and $k_n = n\pi/L$. This choice for the x dependence implies the boundary conditions $\varphi_{1,x}(0) = \varphi_{1,x}(L) = 0$, which is consistent with Eq. (17). The
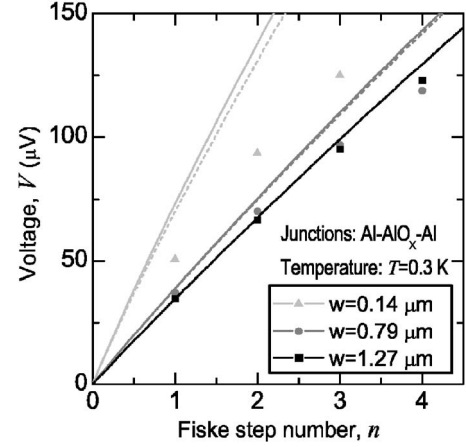

FIG. 13. Comparison of experimentally obtained Fiske step voltages for Al-AlO$_x$-Al junctions of different width (symbols) with the dispersion curve calculated from nonlocal theories taking into account material dispersion (lines). Triangles correspond to the junction of width $w = 0.14$ μm, circles to $w = 0.79$ μm, and rectangles to $w = 0.1.27$ μm. Lines correspond to the theoretical models of edge-type junction neglecting internal nonlocality (Ref. 21) (solid) and to the more general theory describing both internal and geometrical nonlocal effects (Ref. 24) (dashed).

frequency ω_n is determined from the dispersion relation of Eq. (19), namely $\sqrt{\omega^2(k)-\omega_p^2}$, $\omega(k)$ is determined in Sec. IV A. By inserting the expression (20) for φ_1 into Eq. (19), and solving the set of the equations for g_n, we obtain the following expression for the position of the Fiske resonances

$$V_n = \frac{\Phi_0}{2\pi}\sqrt{\omega^2(k_n) - \omega_p^2}. \qquad (21)$$

In the local case, where $Q(x) = \delta(x)$, and $\omega^2(k) = \omega_p^2 + \bar{c}k^2$, we obtain Eq. (6).

Using Eqs. (11), (12), (14)–(16), and (21), in Fig. 10 we plot the dependence of the first Fiske step voltage V_1 on the junction width w for Al-AlO$_x$-Al junctions, and in Fig. 12 for Nb-AlO$_x$-Nb junctions. The only fitting parameter for all curves is the Swihart velocities in the wide junction limit. For the Al-AlO$_x$-Al junctions we found $\bar{c} \simeq 5 \times 10^6$ m/s and for Nb-AlO$_x$-Nb junctions $\bar{c} \simeq 7 \times 10^6$ m/s. The Swihart velocity found using the theory of case[21] (c) and of case[24] (d) differ by about 1%. This small difference indicates that internal nonlocal effects, taken into account in case (d), are negligibly small in our junctions.

In Figs. 13 and 14 we compare the measured (symbols) voltage positions V_n of the Fiske steps to theoretical curves calculated from Eqs. (11), (12), (14)–(16), and (21), where both nonlocality and material dispersion have been taken into account. Solid lines correspond to the theory of case[21] (c), and dashed lines to the theory of case[24] (d). The data for Al junctions is presented in Fig. 13, and for Nb junctions presented in Fig. 14. The difference between the curves according to the two theories decreases with the width of the junctions. For the Nb-AlO$_x$-Nb junction of width 4.2 μm the difference cannot be distinguished. Thus our experimental
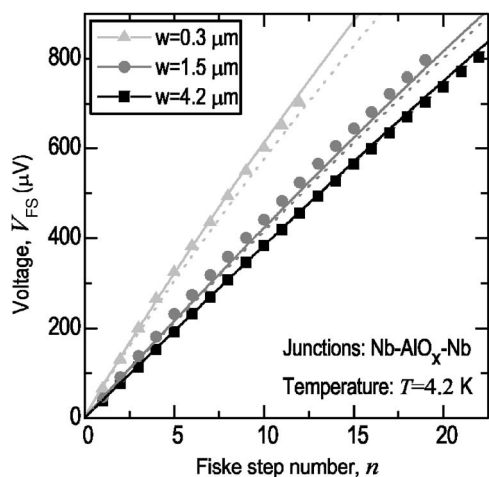
FIG. 14. Comparison of experimentally obtained Fiske step voltages for Nb-AlO$_x$-Nb junctions of different width (symbols) with the dispersion curve calculated from nonlocal theories taking into account material dispersion (lines). Triangles correspond to the junction of width $w=0.3$ μm, circles to $w=1.5$ μm, and rectangles to $w=4.2$ μm. Lines correspond to the theoretical models of edge-type junction neglecting internal nonlocality (Ref. [21]) (solid) and the more general theory describing both internal and geometrical nonlocal effects (Ref. [24]) (dashed).

data for Fiske steps in both Al-AlO$_x$-Al and Nb-AlO$_x$-Nb junctions are in good agreement with theory.

Our estimations show that for Nb junctions the corrections due to material dispersion are about 4 μV, which is about 15% of the spacing between the steps. For the most narrow Al junctions this difference is about 20 μV (40%), and for the widest junction it is about 6 μV (20%).

D. Critical magnetic fields and vortex size

For a junction placed in an external magnetic field the integrodifferential equation (4) contains an additional Meissner current $j_m(x,y,z)$, which also would be induced in the absence of the junction and depends on the size and the shape of the electrodes demagnetization effects. If the dynamics of the phase inside a small surface region of size $\sim\lambda_L \ll L, \widetilde{\lambda}_J$ is disregarded, the geometry dependent current j_m can formally be taken into account by supplying the nonlocal wave equation for the case of infinite length with appropriate nonlocal boundary conditions. Physically, these boundary conditions reflect edge capacitances and inductances, and take into account the stray field in the xy plane for $-w/2 \leq z \leq w/2$, in addition to the stray fields above and below the superconducting leads, which are contained in the nonlocal kernel $Q(x)$. These boundary conditions depend on the geometry of the sample, the magnetic screening length and kernel Q. The magnetic penetration field H_{c1} is therefore more difficult to theoretically estimate than the Fiske steps, whose voltages can be calculated from the kernel Q alone.

Although in general the solution is difficult to find, in the physically relevant case (c) for $\lambda_L \ll \widetilde{\lambda}_J$, where Eq. (4) transforms into the local sine-Gordon equation with a characteristic length $\widetilde{\lambda}_J$, the expressions for H_{c1} and $\bar{c}=\omega_p\lambda_J$ from the

local theory can be used. In doing so the correct magnetic screening length, e.g., λ_L for $w \gtrsim \lambda_L$, and the characteristic length $\widetilde{\lambda}_J=\lambda_J(1+\lambda_L/w)^{1/2}$ from the effective local theory has to be used. Assuming that bulk material properties like j_c do not depend on the junction width w, it is possible to obtain the relationship[10]

$$\bar{c}(w) \sim \frac{1}{H_{c1}^{1/3}(w)}, \qquad (22)$$

which is in agreement with experiment.[10] Even though the effective local theory provides a good approximation to the static case, it might nevertheless fail to describe some significant properties of the junction in the dynamic case, such as the possibility of Cherenkov radiation above a critical velocity (similarly to the internal nonlocality [23]).

We will now verify the correct choice of the characteristic length $\widetilde{\lambda}_J$. Note that the characteristic length $\widetilde{\lambda}_J$ at which the Josephson phase changes is equivalent to the size of a Josephson vortex, and, in the following, they are used as synonyms. Thus the problem is to find how the vortex size changes with junction width. For this purpose we use a variational approach, with the variation parameter being the vortex size $\widetilde{\lambda}_J$, and minimize the Lagrange function of the unperturbed ($\alpha=\gamma=0$) nonlocal sine-Gordon equation (4),

$$\frac{\mathcal{L}}{E_J w} = \int dx\left(\frac{1}{2}\frac{1}{\omega_p^2}\varphi_t^2 - (1-\cos\varphi)\right)$$
$$-\frac{1}{2}\lambda_J^2 \int dxdy\,\varphi_x(x)\varphi_y(y)Q(x-y). \qquad (23)$$

As trial functions we took the two limiting solutions of Eq. (4). For $w \to \infty$, the vortex solution of Eq. (4) is an exponential kink,[37]

$$\varphi(x,\widetilde{\lambda}_J) = 4\arctan\left(\exp\frac{x}{\widetilde{\lambda}_J}\right), \qquad (24)$$

In the other limit $w \to 0$, the single vortex solution decays algebraically:[28]

$$\varphi(x,\widetilde{\lambda}_J) = 2\arctan\frac{x}{\widetilde{\lambda}_J} + \pi. \qquad (25)$$

Here $\widetilde{\lambda}_J$ is considered as a free variational parameter corresponding to the size of the vortex. The results calculated from the first critical field H_{c1} at $T=0.3$ K for Al-AlO$_x$-Al junctions are presented in Fig. 8 by symbols. The lines correspond to variational results for the theories of Refs. 21 and 24 with the above two *Ansätze*. Each curve was fitted to the experimental data. The prefactors for different theories differ by 3%. Figure 11 presents the vortex size $\widetilde{\lambda}_J$ as a function of junction width for Nb-AlO$_x$-Nb junctions, for $T=4.2$ K. In this figure the curves are fitted to the experimental data point at width $w=4.2$ μm. One notes that in both cases all four curves overlap with each other.

The agreement between experimental data (symbols) and theoretical estimations (lines) in Figs. 11 and 8 is only qualitative. We suppose this is due to the fact that none of the

theories properly consider the boundary conditions at the edges of a junction. Deriving appropriate boundary conditions for realistic junction geometries in the nonlocal case remains an unsolved problem, which requires further work.

E. Vortex mass

Finally, we would like to discuss the effect of nonlocal electrodynamics on the dynamical mass and the quantum behavior of Josephson vortices. We note that the first experiment with a vortex in the quantum regime was presented in Ref. 5. The nonrelativistic mass m_F of a Josephson vortex, which appears in the equation of motion

$$m_F \ddot{q} + \frac{\partial \mathcal{H}_{\text{ext}}}{\partial q} = 0 \qquad (26)$$

for the vortex center of mass coordinate q in an external potential $\mathcal{H}_{\text{ext}}$, is obtained by expanding the Lagrange function

$$\mathcal{L} \approx \frac{1}{2} m_F v^2 - H_{\text{ext}} + \text{const} \qquad (27)$$

of Eq. (23) in terms of $v \ll \bar{c}$. The spacing $\hbar \omega_0$ between the energy levels (and thus zero-point fluctuations) is then given by

$$\omega_0^2 = \frac{1}{2 m_F} \frac{\partial^2 H_{\text{ext}}}{\partial q^2}. \qquad (28)$$

The condition $\hbar \omega_0 > k_B T$ is required for dominantly quantum behavior of the fluxon. In the limit $m_F \to 0$, the spectrum becomes discrete, provided that the energy scale of the potential is fixed.

The external potential $\mathcal{H}_{\text{ext}}$ for a vortex in a Josephson junction can be, for example, induced by an external magnetic field or by the presence of a microshort or microresistor. In the first case, the external magnetic field creates a screening current flowing through the junction. Provided that the nonlocality of the magnetic screening at the edges can be neglected or, equivalently, Eq. (17) for the boundary condition is justified, the current spreads homogenously over the width of the junction. Hence the external potential $\mathcal{H}_{\text{ext}}$ is proportional to the junction width.[38] In the second case, the inhomogeneity leads to a local change in the Josephson energy. If the magnitude of the inhomogeneity is constant across the junction, the total change in the Josephson energy is proportional to w. As we see, in both situations the external potential $\mathcal{H}_{\text{ext}}$ scales with w hence for characterizing the degree of quantum behavior, the use of the *specific* mass $\tilde{m}_F = m_F/w$ for a vortex is more appropriate than using the mass m_F.

For local theory $(\lambda_J \gg w \gg \lambda_L)$, the mass of a vortex of the form (24) is given by

$$m_F = \frac{8 E_J w}{\omega_p^2 \lambda_J}, \qquad (29)$$

which vanishes in the limit $w \to 0$, whereas the specific mass $\tilde{m}_F = m_F/w$ is constant. In Eq. (29), the Josephson energy E_J is given by $E_J = \frac{\Phi_0 j_c \lambda_J}{2\pi}$.

Similarly, in the nonlocal case we make use of the *Ansatz* $\phi(x,t,v) = \tilde{\phi}(\tilde{x},v)$, where $\tilde{x} = (x - vt)/\tilde{\lambda}_J(v)$ and $\tilde{\lambda}_J(v)$ is the size of the vortex, which in general depends on the velocity [cf. the Lorentz-factor $1/\sqrt{1 - (v/\bar{c})^2}$ in the local case], and which can be determined from the variational *Ansatz*. As the Lorentz invariance is broken in the nonlocal case, we do not know *a priori* the functional dependence of ϕ on v, and an additional explicit dependence on v is possible, if the shape of the vortex depends on v. From Eq. (23) we obtain

$$\frac{\mathcal{L}}{E_J w} = \frac{1}{2\omega_p^2} \frac{1}{\tilde{\lambda}_J} I_1 v^2 + \tilde{\lambda}_J I_2 + \frac{\lambda_J^2}{2} I_3(\tilde{\lambda}_J(v), \lambda_L, w), \qquad (30)$$

where

$$I_1 = \int d\tilde{x}\, (\tilde{\varphi}'(\tilde{x}))^2; \qquad (31)$$

$$I_2 = -\int d\tilde{x}(1 - \cos \tilde{\varphi}); \qquad (32)$$

$$I_3 = -\int d\tilde{x}d\tilde{y}\tilde{\varphi}'(\tilde{x})\tilde{\varphi}'(\tilde{y})Q(\tilde{\lambda}_J|\tilde{x} - \tilde{y}|). \qquad (33)$$

The effective mass in the nonlocal case is obtained by expanding $\mathcal{L}(v)$ into second order. Neglecting the explicit dependence on v, and expanding

$$\tilde{\lambda}_J(v) = \tilde{\lambda}_{J0} + \frac{1}{2} \frac{d^2 \tilde{\lambda}_J}{dv^2} v^2 = \tilde{\lambda}_{J0} + \frac{1}{2} \frac{v^2}{\bar{c}^2}, \qquad (34)$$

one obtains

$$m_f = \frac{E_J w}{\omega_p^2} \frac{I_1}{\tilde{\lambda}_{J0}} + \frac{E_J w}{2} \frac{d^2 \tilde{\lambda}_J}{dv^2} \left(2I_2 + \lambda_J^2 \frac{\partial I_3(\tilde{\lambda}_J = \tilde{\lambda}_{J0})}{\partial \tilde{\lambda}_J} \right). \qquad (35)$$

Here we again apply the variational approach to obtain the vortex size. Then the expression in brackets is the Lagrange equation for the variational parameter $\tilde{\lambda}_{J0}$, and is therefore equal to zero. Thus the effective mass for the trial function of the form (24) can explicitly be written as

$$m_f = \frac{8 E_J w}{\omega_p^2 \tilde{\lambda}_{J0}}. \qquad (36)$$

Since $\tilde{\lambda}_J$ is larger for more narrow junctions, both the effective mass m_f and the specific mass m_f/w, which is responsible for the energy scaling if $\mathcal{H}_{\text{ext}} \sim w$, decrease with decreasing junction width. From Eq. (36) one notes that the inverse of the specific mass scales with the vortex size $\tilde{\lambda}_{J0}$ (see Figs. 8 and 11).

Let us emphasize again that the possibility of a vortex behaving as a macroscopic quantum particle, when reducing the width w of the junction, not only depends on the scaling of the kinetic mass m_F, but more exactly the ratio of the kinetic energy to the external potential $\mathcal{H}_{\text{ext}}$, which has to be determined for each specific experimental situation.

The static mass of a fluxon corresponds to the energy of a junction with one trapped fluxon. Hence by calculating the fluxon mass, we can find out how large the energy of the stray fields is. Our estimations for the 0.5-μm-wide Nb junction show that the stray field energy is about half of the internal energy, or about 30% of the total energy.

V. CONCLUSION

The measured current-voltage characteristics and the critical current vs field patterns of narrow long Josephson junctions show a strong dependence on the junction width w. This behavior cannot be explained using the conventional theory based on the local sine-Gordon model. Our experimental data are well described by the nonlocal theory originally developed by Ivanchenko,[21] and later extended by Lomtev and Kuzovlev.[24] According to these models, the electrodynamic and static properties of a junction depend on the junction width. Our experimental data for Fiske steps observed in both Al-AlO$_x$-Al and Nb-AlO$_x$-Nb long narrow junctions are in rather good quantitative agreement with these theories. The dependence of the first critical field on the width of the junction allows qualitative estimates of the characteristic vortex size, which is influenced by nonlocal effects. A proper description of the static effects requires a better treatment of the boundary conditions at the edges of a junction. For our junctions the geometric nonlocal effects become important when junctions are a few London penetration depths wide.

We also calculated the specific mass of a vortex in the nonlocal case. According to local theory, the specific mass does not depend on the junction width w. By contrast, the nonlocal theory predicts that the specific mass of a vortex decreases with decreasing junction width. The static mass of a vortex is proportional to electromagnetic field energy. Hence the junction energy in the nonlocal case decreases with decreasing junction width faster than a linear function.

ACKNOWLEDGMENTS

*Electronic address: abdumalikov@physik.uni-erlangen.de

[1] I. O. Kulik and I. K. Yanson, *The Josephson Effect in Superconducting Tunnel Structures* (Keter Press, Jerusalem,1972).

[2] A. Barone and G. Paternó, *Physics and Applications of the Josephson Effect* (Wiley, New York, 1982).

[3] K. K. Likharev, *Dynamics of Josephson Junctions and Circuits* (Gordon and Breach, New York, 1986).

[4] A. V. Ustinov, Physica D **123**, 315 (1998).

[5] A. Wallraff, A. Lukashenko, J. Lisenfeld, A. Kemp, M. V. Fistul, Y. Koval, and A. Ustinov, Nature (London) **425**, 155 (2003).

[6] M. V. Fistul, A. Wallraff, Y. Koval, A. Lukashenko, B. A. Malomed, and A. V. Ustinov, Phys. Rev. Lett. **91**, 257004 (2003).

[7] Z. Hermon, A. Stern, and E. Ben-Jacob, Phys. Rev. B **49**, 9757 (1994).

[8] T. Kato and M. Imada, J. Phys. Soc. Jpn. **65**, 2963 (1996).

[9] A. Shnirman, E. Ben-Jacob, and B. Malomed, Phys. Rev. B **56**, 14677 (1997).

[10] Y. Koval, A. Wallraff, M. Fistul, N. Thyssen, H. Kohlstedt, and A. V. Ustinov, IEEE Trans. Appl. Supercond. **9**, 3957 (1999).

[11] D. C. Mattis and J. Bardeen, Phys. Rev. **111**, 412 (1958).

[12] G. S. Lee and A. T. Brafknecht, IEEE Trans. Appl. Supercond. **2**, 67 (1992).

[13] M. Tinkham, *Introduction to Superconductivity*, 2nd ed. (McGraw-Hill, New York, 1996).

[14] A. Gurevich, Phys. Rev. B **46**, R3187 (1992).

[15] Y. M. Aliev, V. P. Silin, and S. A. Uryupin, J. Supercond. **5**, 1992 (1992).

[16] G. M. Lapir, K. K. Likharev, L. A. Maslova, and V. K. Semenov, Fiz. Nizk. Temp. **1**, 1235 (1975) [Sov. J. Low Temp. Phys. **1**, 590 (1975)].

[17] M. Y. Kupriyanov, K. K. Likharev, and V. K. Semenov, Fiz. Nizk. Temp. **2**, 706 (1976) [Sov. J. Low Temp. Phys. **2**, 346 (1976)].

[18] Y. M. Ivanchenko and T. K. Soboleva, Phys. Lett. A **147**, 65 (1990).

[19] V. G. Kogan, Phys. Rev. B **49**, 15874 (1994).

[20] N. Thyssen, A. V. Ustinov, H. Kohlstedt, J. G. Caputo, S. Pagano, and N. Flytzanis, in *Proceedings of the International Conference on Nonlinear Superconducting Devices and High-Tc Materials*, edited by R. D. Parmentier and N. F. Pedersen (World Scientific, Singapore, 1994).

[21] Y. M. Ivanchenko, Phys. Rev. B **52**, 79 (1995).

[22] R. G. Mints and I. B. Snapiro, Phys. Rev. B **51**, 3054 (1995).

[23] R. G. Mints and I. B. Snapiro, Phys. Rev. B **52**, 9691 (1995).

[24] Y. E. Kuzvovlev and A. I. Lomtev, JETP **84**, 986 (1997).

[25] A. I. Lomtev, JETP **86**, 1234 (1998).

[26] J. G. Caputo, N. Flytzanis, V. V. Kurin, N. Lazarides, and E. Vavalis, J. Appl. Phys. **85**, 7282 (1999).

[27] N. Flytzanis, N. Lazarides, A. Chiginev, V. V. Kurin, and J. G. Caputo, J. Appl. Phys. **88**, 4201 (2000).

[28] V. G. Kogan, V. V. Dobrovitski, J. R. Clem, Y. Mawatari, and R. G. Mints, Phys. Rev. B **63**, 144501 (2001).

[29] N. Grønbech-Jensen and M. R. Samuelsen, Phys. Rev. B **65**, 144512 (2002).

[30] J. Pearl, Appl. Phys. Lett. **5**, 65 (1964).

[31] G. J. Dolan, Appl. Phys. Lett. **31**, 337 (1977).

[32] *Handbook of Mathematical Functions with Formulas, Graphs, and Mathematical Tables*, edited by M. Abramowitz and A. Stegun (U.S. GPO, Washington, D.C., 1965).

[33] H. Hilgenkamp and J. Mannhart, Rev. Mod. Phys. **74**, 485 (2002).

[34] I. O. Kulik, JETP Lett. **2**, 84 (1965).

[35] I. O. Kulik, Sov. Phys. Tech. Phys. **12**, 111 (1967).

[36] A. A. Abdumalikov, Jr., and V. V. Kurin (unpublished).

[37] G. L. Lamb, *Elements of Soliton Theory* (Wiley, New York, 1980).

[38] N. Martucciello and R. Monaco, Phys. Rev. B **53**, 3471 (1996).